SLAC-TN-70-1
H. Brechna
January 1970

TESTING OF A LARGE-VOLUME, 10-T, COMPOSITE SUPERCONDUCTING COIL SYSTEM

Summary

A coil system, consisting of 7 independent solenoid modules with a bore diameter of 18.6 cm, a uniform field length of 25 cm, was tested at 4.2° K to study its charging and steady-state behavior. The 6 outer modules, with a bore diameter of 30 cm and overall length of 70 cm, provided the backing field of 5.7 T, while the inner module provided an additional 4.2 T. The central field of 9.9 T was reached, which corresponds to a total field energy of 4.5 Mjoules. The maximum field at the inner coil diameter exceeded 10.3 T. The inner module is composed of 16 pancakes of Nb_3Sn. The outer 6 modules are composite cables, based on Nb_xTi and Nb_xZr, and copper conductors. The steady-state helium boil-off of the total system was approximately 8 liters per hour, while the static boil-off did not exceed 4 liters per hour. The total weight of the coil system and support structure to be cooled to 4.2° K is 1620 kg.

I. INTRODUCTION

The main reason for SLAC to test and evaluate the performance of a high-field solenoid to be used as part of the bubble-chamber magnet system at CERN for measuring the magnetic moment of Σ^+ hyperons was that at the time of magnet testing at SLAC, only part of the bubble-chamber magnet system was in existence. SLAC has also a working magnet which can accommodate this part and the SLAC facility is convenient to operate for high-energy superconducting systems. The high-field performance of this Nb_3Sn solenoid must be first tested before the rest of the magnet system (5 modules based on stabilized Nb_xTi composite conductor) can be wound directly on the coil. This insert coil was supposed to produce by itself a field in excess of 4 T, while the whole magnet system must generate a field of 11 - 12 T within a bore of 0.186 m diameter.

The insert solenoid has a diameter of 0.186 m and a length of 0.25 m, while the useful part of the bubble chamber consists of a cylinder of 0.128 m diameter and 0.32 m axial length.

The method of measuring the magnetic moment of Σ^+ is the same as performed in earlier experiments. It measures the amount of precession of the hyperon polarization in a magnetic field during the lifetime (10^{-10} sec) of the hyperon.

This experiment was planned due to measurement errors of previous experiments. Systematic errors such as:

(a) poor measurement accuracy, errors in position, momentum, field

made it practically impossible to measure the magnetic moment to ± 0.2 nuclear magneton. To improve measurement accuracy, one may choose the following methods:

(a) The accuracy of angular measurements can be improved in a spark chamber experiment.

(b) Improve the statistics in an evaluation experiment.

(c) Utilize a small volume bubble chamber operating in a high magnetic field.

The last method was adopted by the group at Max Planck Institute in Munich and Vanderbilt University in Nashville, Tennessee.[1]

The bubble chamber magnet system is designed such that over 0.24 m axial bubble chamber length, the axial magnetic field varies between 10 T - 12 T and drops from 10 T to 6 T over the rest of the bubble chamber. The precession of the hyperon polarization will be measured in the high field region. Hyperon decay products are analyzed in the region of the high gradient field.

The polarized Σ^+ will be produced in the reaction

$$K^- p \longrightarrow \Sigma^+ \pi^- \ .$$

The Σ^+ polarization is observed in the

$$\Sigma^+ \longrightarrow p \pi^o$$

decay angular distribution.

It is hoped that with the high field system, the statistical accuracy achieved will be below the magnitude of systematic effects. The measurement accuracy should be an order of magnitude better than in previous spark chamber experiments.

For the experiment, 6×10^5 pictures will be taken and 3×10^4 events measured.

The insert coil has an outer diameter of 0.258 m and thus the SLAC 0.3-m magnet was well suited to test the performance of this coil before the outer coils were wound on it.

The basic idea was to produce an external field of ~ 6 T by means of the SLAC coil[2] and generate a self field of 4 T - 5 T with the insert coil at the center of the magnet.

During the experiment, the SLAC magnet produced a central field of 5.7 T and the insert coil, a field of 4.2 T. After several runs, it was decided not to increase the external field (SLAC coil) due to the possibility of an eventual quench in module II and the unavailability of additional liquid helium which would have made successive runs impossible. However, the fear was not justified, specifically because all the quenches occurred in the insert coil (module IV)* which, of course, triggered the field decay over the entire coil system. As the field at the conductor (insert coil) was higher than 10.3 T, it was accepted by all parties concerned that the experiment was a success.**

The total magnet system at 10 T had a field energy of 4.5 Mjoules. When the magnet did quench at a central field of 9.9 T, the energy dissipated within the helium container evaporated 151 liters of helium, corresponding to 0.4 Mjoule. The evaporated gas was entirely captured in the closed circuit helium system and no helium was lost.

With a backing external field of 6 T or higher, the insert coil carries a transport current which is approximately of short-sample value.

---

*Module IV, based on partially stabilized Nb_3Sn tape, was built by General Electric Company, Schenectady, New York.

**During the last test, Professor Charles Roos of Vanderbilt, Dr. V. Scheuing of Max Planck Institute, and Mr. E. Mains of General Electric were present to witness the tests.

II. MAGNET SYSTEM CONFIGURATION

The magnet assembly is illustrated in Fig. 1, and consists of 7 modules, with 6 modules forming a split-coil arrangement (I ... III). They do generate the external magnetic field (backing field) for the inner module IV. Detail data of the external magnet are given elsewhere.[2] In this test, coils I and III were energized from one current-regulated power supply and connected in series. Modules II and IV are energized separately.

Coil II, consisting of a single superconductive core, is unstable and was energized only to $\sim$ 0.3 T to prevent premature coil quenching experienced during earlier tests.

The insert coil (module IV) was placed inside the SLAC split-coil arrangement such as to obtain best possible superposition of the geometrical centers.

It was realized that both coil sections are far from ideal. Each individual coil section will have magnetic centers different from geometric centers.

The principal problem which had to be met in the helium container is the support of the interaction forces between Module IV and Coil (I ... III). Even coil (I ... III) is far from being perfectly aligned.

To obtain some idea of the magnitude of forces parallel and perpendicular to the coil axis, we assume the coil axis as being parallel and the coil centers as being displaced by a distance (s) in the radial and by d in the axial direction (Fig. 2).

We calculate the mutual inductance between the two coils. The partial derivatives with respect to s and with respect to d will give the forces perpendicular and parallel to the coil axis.

The mutual inductance of coils displaced radially and axially was derived by Dwight and Pursell[3] and modified by Grover:[4]

$$M = \pi^2 \cdot a_1^2 \cdot a_2^2 \cdot \frac{N_1 \cdot N_2}{b_1 \cdot b_2} \left[\frac{Z_1}{r_1} - \frac{Z_2}{r_2} - \frac{Z_3}{r_3} + \frac{Z_4}{r_4}\right] \times 10^{-9} \quad \text{(H)} \qquad (1)$$

in which the coil dimensions are given in cm and the quantity:

$$\begin{aligned} Z_m = {} & T_2 t_2 - \frac{1}{4} \cdot \frac{a_2^2}{r_m^2} \left[T_4 t_2 + \left(\frac{a_1}{a_2}\right)^2 \cdot T_2 t_4\right] \cdot P_2 (\cos\theta) \\ & + \frac{1}{8} \cdot \left(\frac{a_2}{r_m}\right)^4 \cdot \left[T_6 t_2 + 3\left(\frac{a_1}{a_2}\right)^2 \cdot T_4 t_4 + \left(\frac{a_1}{a_2}\right)^4 \cdot T_2 t_6\right] P_4 (\cos\theta) \\ & - \frac{5}{64} \left(\frac{a_2}{r_m}\right)^6 \left[T_8 t_2 + 6\left(\frac{a_1}{a_2}\right)^2 \cdot T_6 t_4 + 6\left(\frac{a_1}{a_2}\right)^4 \cdot T_4 t_6 + \left(\frac{a_1}{a_2}\right)^6 \cdot T_2 t_8\right] P_6 (\cos\theta) \\ & + \frac{7}{128} \left(\frac{a_2}{r_m}\right)^8 \left[T_{10} t_2 + 10\left(\frac{a_1}{a_2}\right)^2 \cdot T_8 t_4 + 20\left(\frac{a_1}{a_2}\right)^4 \cdot T_6 t_6 + 10\left(\frac{a_1}{a_2}\right)^6 \cdot T_4 t_8 \right. \\ & \left. + \left(\frac{a_1}{a_2}\right)^8 \cdot T_2 t_{10}\right] P_8 (\cos\theta) \\ & - \ldots . \\ & + \ldots . \end{aligned} \qquad (2)$$

In Eq. (2):

$$r_m = \left(\delta_m^2 + \tau_n^2\right)^{1/2}$$

and

$$\delta_1 = d - \left(\frac{b_1 + b_2}{2}\right)$$

$$\delta_2 = d + \left(\frac{b_1 - b_2}{2}\right)$$

$$\delta_3 = d - \left(\frac{b_1 - b_2}{2}\right)$$

$$\delta_4 = d + \left(\frac{b_1 + b_2}{2}\right)$$

$P_{2n}(\cos\theta)$ are the zonal harmonics for arguments of $\cos\theta = \frac{d_m}{r_m}$. The factors t_2, t_4 ... are expressed as:

$$t_n = 1 + \frac{n(n-1)}{3!}\,\frac{\tau^2}{2^2} + \frac{n(n-1)(n-2)(n-3)}{5!}\cdot\frac{\tau^4}{2^4}$$

$$+ \ldots \frac{n(n-1)(n-2)(n-3)\ldots.\left[n-(n-1)\right]}{(n+1)!}\cdot\frac{\tau^n}{2^n} \qquad (3)$$

with:

$$\tau^2 = \left(\frac{t}{a_1}\right)^2$$

Replacing t by T, we obtain for $\tau^2 = \left(\frac{T}{a_2}\right)^2$ to calculate T_n from Eq. (3).

Equation (2), although useful to calculate mutual inductance of coils with magnetic centers located at any place in space with respect to each other, has one drawback which makes it practically useless for coils located eccentrically inside each other, or separated axially with common axes.

Equation (2) is convergent only if

$$r_m > a_1 + a_2 \quad .$$

This is certainly not true if s and d are small compared to a_1 and a_2, which is the case with magnet coils composed of several modules.

To calculate the mutual inductance between arbitrarily located coils, one does divide each coil cross-sectional area into a number of equal squares. A current filament carrying a current I_m is located in the center of each square. The mutual inductance of a filament p and all the filaments m of the other coil must be calculated, resulting in m equations. Thus, if the cross section of one coil is divided into n equal squares and the cross section of the other coil into m equal squares, the mutual inductance between the two coils is derived by summing up the mutual inductance of n(m - 1) filaments.

However, a more simplified method, which gives adequate and accurate results, is proposed later, by using Eq. (6) or Eq. (7).

The mutual inductance of a pair of circles located at arbitrary positions with respect to each other but with their symmetry axes being parallel is calculated as follows (Fig. 3):

Using the ratios:

$$\alpha = \frac{a_1}{a_2} \quad , \quad \delta = \frac{d}{a_2} \quad ,$$

the mutual inductance of two displaced circular filaments is given by

$$M = (a_1 \cdot a_2)^{\frac{1}{2}} \int_0^{\pi} \frac{f}{\pi} \frac{\left(1 - \frac{s}{a_1} \cos \phi\right)}{\left[1 - 2 \frac{s}{a_1} \cos \phi + \left(\frac{s}{a_1}\right)^2\right]^{3/4}} \, d\phi \qquad \text{(nH)} \qquad (4)$$

The factor f depends on the dimensions of both circular filaments and is obtained from Fig. 4 as a function of the module k'^2, where:

$$k'^2 = \frac{\left\{1 - \alpha \left[1 - 2\frac{s}{a_1} \cos \phi + \left(\frac{s}{a_1}\right)^2\right]^{1/2}\right\}^2 + \delta^2}{\left\{1 + \alpha \left[1 - \frac{2s}{a_1} \cos \phi + \left(\frac{s}{a_1}\right)^2\right]^{1/2}\right\}^2 + \delta^2} \quad .$$

The integration of Eq. (4) may be performed by mechanical quadrature or by computer calculation. We apply both methods and compare the accuracy of results.

As an example, the mutual inductance between the central filaments of module I-a and IV is calculated (Fig. 1). It was assumed that the magnetic center of module IV is displaced from the theoretical location due to mechanical misalignment by 1 cm in radial direction. The axial displacement between module I-a and IV is assumed to be 34 cm (theoretical value 33 cm), and between I-b and IV, 32 cm.

Thus:

$$\left.\begin{aligned} s &= 1 \text{ cm} \\ a_1 &= 11 \text{ cm} \\ a_2 &= 26.0 \text{ cm} \\ d &= 34 \text{ cm} \end{aligned}\right\} \quad \begin{aligned} \alpha &= 0.4112 \\ \delta &= 1.371 \\ \frac{s}{a_1} &= 0.0909 \end{aligned}$$

We calculate first M between I-a and IV.

For hand calculation, I applied Simpson's formula to solve Eq. (4). The interval of integration is divided into an even number. We choose 15^{o} intervals. If $y_0, y_1 \ldots . y_2$ denote the calculated values of the integrand, then Simpson's formula is written in the form:

$$S = \frac{1}{3}\left(\frac{\pi}{12}\right) \cdot \left[2 \cdot \left(y_0 + y_2 + y_4 + y_6 \cdots y_{12}\right) + 4 \cdot \left(y_1 + y_3 + y_5 + \cdots y_{11}\right) - \left(y_0 + y_{12}\right)\right] \quad (5)$$

If more accuracy is needed, the interval can be subdivided into 24 or 48 parts. With the data given, the complementary modulus is

$$k'^2 = \frac{\left[1 - 0.411\ (1.008 - 0.1818 \cos\phi)^{1/2}\right]^2 + 1.615}{\left[1 + 0.411\ (1.008 - 0.1818 \cos\phi)^{1/2}\right]^2 + 1.615}$$

In the table below, the method of integration is illustrated.

ϕ	k'^2	f	y_n
0	0.572392	10^{-3}	1.057×10^{-3}
15°	0.5739	1.01×10^{-3}	1.0467×10^{-3}
30°	0.5689	1.01×10^{-3}	1.0497×10^{-3}
45°	0.5645	1.05×10^{-3}	1.0825×10^{-3}
60°	0.5572	1.1×10^{-3}	1.12×10^{-3}
75°	0.5496	1.1374×10^{-3}	1.143×10^{-3}
90°	0.495	1.44×10^{-3}	1.44×10^{-3}
105°	0.5356	1.2×10^{-3}	1.179×10^{-3}
120°	0.529	1.244×10^{-3}	1.211×10^{-3}
135°	0.524	1.27×10^{-3}	1.227×10^{-3}
150°	0.520	1.3004×10^{-3}	1.248×10^{-3}
165°	0.5177	1.31×10^{-3}	1.255×10^{-3}
180°	0.517	1.31×10^{-3}	1.253×10^{-3}

From this table, we obtain:

$$y_0 = 1.057 \times 10^{-3}$$
$$y_2 = 1.0497 \times 10^{-3}$$
$$y_4 = 1.12 \times 10^{-3}$$
$$y_6 = 1.44 \times 10^{-3}$$
$$y_8 = 1.211 \times 10^{-3}$$
$$y_{10} = 1.248 \times 10^{-3}$$
$$y_{12} = 1.253 \times 10^{-3}$$
$$\sum_{2n=0}^{12} y_{2n} = 8.3787 \times 10^{-3}$$

$$y_1 = 1.0467 \times 10^{-3}$$
$$y_3 = 1.0825 \times 10^{-3}$$
$$y_5 = 1.143 \times 10^{-3}$$
$$y_7 = 1.179 \times 10^{-3}$$
$$y_9 = 1.227 \times 10^{-3}$$
$$y_{11} = 1.255 \times 10^{-3}$$
$$\sum_{n=0}^{5} y_{2n+1} = 6.904 \times 10^{-3}$$

$$y_0 = 1.57 \times 10^{-3}$$
$$y_{12} = 1.253 \times 10^{-3}$$
$$\sum = 2.310 \times 10^{-3}$$

Thus:

$$S = \frac{\pi}{36} \cdot [42.063] \times 10^{-3}$$

$$\frac{S}{\pi} = 1.1684 \times 10^{-3}$$

The mutual inductance between the filaments $P_{IV,0}$ and $P_{Ia,0}$ is according to Eq. (4):

$$M_0 = \sqrt{a_1 \cdot a_2} \cdot \frac{S}{\pi}$$

$$= (11 \times 26.75)^{1/2} \times 1.1684 \times 10^{-3}$$

$$= 2.00497 \times 10^{-8} \text{ H.}$$

The simplest method to obtain the mutual inductance between the modules (IV) and (Ia) is to multiply M_0 with the number of turns of the two coils:

$$\begin{aligned} M &= N_{IV} \cdot N_{Ia} \cdot M_0 \\ &= 2.399 \times 10^3 \times 2.07 \times 10^3 \times 2.00497 \times 10^{-8} \\ &\cong 10 \times 10^{-2} \text{ H} \end{aligned}$$

As the main radii of the two coils are appreciable, compared to the distances between the coils, the mutual inductance obtained this way is too small, since the turns in the portions of the coils adjacent to each other would contribute much more than is compensated for by contribution of the turns at the far portions of the coils. A better result is obtained from the following equation:

$$M = \frac{N_1 N_2}{6} \left[\left(M_{01'} + M_{02'} + M_{03'} + M_{04'} \right) + \left(M_{0'1} + M_{0'2} + M_{0'3} + M_{0'4} \right) - 2 M_{00'} \right] \tag{6}$$

The mutual inductance of each pair of filaments is calculated from Eq. (4).

Repeating the calculation procedure as shown above, the mutual inductance between coils Ia and IV was calculated to be:

$$M_{IV,Ia} = 0.292 \text{ H.}$$

In the same manner, we obtained the mutual inductance between the SLAC-Max Planck coil, for all 7 modules, if IV is axially displaced by 1 cm:

$$M_{IV\text{-SLAC}} = 1.357 \text{ H} .$$

The mutual inductance between the solenoid IV and the other modules (I ... III), if the axial and radial displacements are zero, may be calculated, using equations of M for coaxial circular filaments and using Eq. (6) to obtain M for the whole system.

However, the particular case of three sets of coaxial coils with pairs of identical coils (a - b) is simplified as:

$$M = \frac{N^2}{3}\left(M_{01} + M_{02} + M_{03} + M_{04} - M_{00'}\right). \tag{7}$$

The mutual inductance of a pair of circles with the radii a_1 and a_2, located at a distance d is given by

$$M = f \cdot \left(a_1 \cdot a_2\right)^{1/2} \quad . \tag{8}$$

The factor f was given in Fig. 4 as a function of k'^2 :

$$k'^2 = \frac{\left(a_2 - a_1\right)^2 + d^2}{\left(a_2 + a_1\right)^2 + d^2} = \frac{\left(1 - \frac{a_1}{a_2}\right)^2 + \left(\frac{d}{a_2}\right)^2}{\left(1 + \frac{a_1}{a_2}\right)^2 + \left(\frac{d}{a_2}\right)^2} \quad . \tag{9}$$

If the circles are very close together ($k'^2 \leqq 0.1$), we see from Fig. 4 that f is nearly proportional to $\log_{10}\left(k'^2\right)$. One may use the relation:

$$f = 1.4468 \times 11^{-2}\left[\log_{10}\left(\frac{1}{k'^2}\right) - 0.53307\right] . \tag{10}$$

For greater accuracy, the value of f may be computed from Maxwell's[5] equation:

$$M = 4\pi\left(a_1 \cdot a_2\right)^{1/2}\left\{\left(\frac{2}{k} - k\right)K(k) - \frac{2}{k}E(k)\right\} \tag{11}$$

with

$$k^2 = \frac{4 a_1 a_2}{\left(a_1 + a_2\right)^2 + d^2}$$

the complementary modulus of

$$k'^2 = \frac{(a_2 - a_1)^2 + d^2}{(a_2 + a_1)^2 + d^2}$$

given in Eq. (9). K and E are the complete elliptic integrals of the first and second kinds, respectively.

If the coaxial circles are too close, Eq. (11) is not accurate. We may use Weinstein's[6] famous formula:

$$M = 4\pi (a_1 \cdot a_2)^{\frac{1}{2}} \cdot \left\{ \left(1 + \frac{3}{4}k'^2 + \frac{33}{64}k'^4 + \frac{107}{256}k'^6 + \frac{5913}{16384}k'^8 + \ldots\right) \cdot \left[\frac{1}{2}\ell n\left(\frac{16}{k'^2}\right) - 1\right] \right.$$

$$\left. - \left(1 + \frac{15}{128}k'^4 + \frac{185}{1536}k'^6 + \frac{7465}{65536}k'^8 + \ldots\right) \right\} \quad . \tag{12}$$

For $k' < 1$, Weinstein's equation is rapidly convergent.

Using Eq. (11), (12), and (6), the mutual inductance between coils I ... IV are calculated:

$$M_{IV,(I\ldots III)} = 1.386 \quad H.$$

Comparing this value to M for a displaced coil, we obtain from the difference in energy in axial and radial directions, the axial:

$$dF_a = \frac{\partial M_a}{\partial \delta} \cdot I_1 I_2 \cong I_1 \cdot I_2 \cdot \frac{\Delta M_a}{\Delta \delta} \quad , \tag{13}$$

and:

$$\Delta F_s \cong I_1 \cdot I_2 \cdot \frac{\Delta M_s}{\Delta s} \quad , \tag{14}$$

the radial restoring forces.

For $I_1 = 500$ A, $I_2 = 500$ A, $N_I = 2.399 \times 10^3$, $N_{SLAC} \cong 8.28 \times 10^3$ turns, which corresponds to $\sim$ 10 T central field, and assuming that the displacements were 10^{-2} m in axial and radial directions, respectively, we obtain the axial spring constant of

$$F_a = 15 \times 10^5 \text{ N/m}$$

and the radial spring constant of

$$F_s = 4.4 \times 10^5 \text{ N/m} \quad .$$

The axial force is a restoring force. Proper coil alignment and the allowance of some relative axial motion would not cause any damage.

The radial force, however, is not a restoring force and the conditions are of unstable equilibrium. If the magnetic centers are displaced, accelerating forces are introduced.

In our particular case, the radial displacement was less than 0.2 cm and the axial displacement less than 0.5 cm.

The support of the inner solenoid IV, with respect to the SLAC coil, was designed according to the calculated values given above, which proved to be adequate.

The above calculations of M are not for the most general cases. One may also calculate the mutual inductance between displaced coils having inclined axes in the same way as indicated by Eq. (4).

Grover[7] gives a general formula for filaments with axes inclined by the angle θ:

$$M = \left(a_1 \cdot a_2\right)^{\frac{1}{2}} \cdot \cos\theta \int_0^{\pi} \cdot \frac{f}{\pi} \frac{d\phi}{\left(1 - \sin^2\theta \cos^2\phi\right)^{3/4}} d\phi \qquad \text{(nH)} \qquad (15)$$

f is given in Fig. 4 as a function of the module k'^2, expressed as:

$$k'^2 = \frac{1 + \alpha^2 + \delta^2 + 2\alpha\delta\cos\phi\cos\theta - 2\alpha\left(1 - \sin^2\theta\cos^2\phi\right)^{1/2}}{1 + \alpha^2 + \delta^2 + 2\alpha\delta\cos\phi\cos\theta + 2\alpha\left(1 - \sin^2\theta\cos^2\phi\right)^{1/2}}$$

The mutual inductance of inclined coils may be calculated from Eq. (6).

The coil self inductance was calculated in an earlier paper,[8] and may be used in combination with the mutual inductance values obtained here to determine the coil total field energy, which for our case is 4.5×10^6 joules.

III. MAGNET COOL-DOWN AND HELIUM BOIL-OFF

The weight of the whole system, including the insert coil and the support structure, is 1620 kg, of which 1060 kg is the weight of copper and superconductor (Nb_3Sn in the Max Planck coil, Nb(50%)Ti in the SLAC coil), 350 kg stainless steel, 140 kg aluminum, and 70 kg of insulation and miscellaneous metals and materials. To cool down this mass from 300° K to 4.2° K, a total of 1.11×10^8 joules must be removed from the magnet. With the SLAC refrigeration system (7-watt liquefier, operated as a refrigerator, yields $\sim$ 20 watts at 4.5° K), this cool-down can be accomplished at a slow rate of an average of 3° K per hour. We decided to cool down the magnet system by using supplementary gaseous and liquid nitrogen, which was pumped through a built-in heat exchanger within the coil modules.

The coil and insulation are cooled by conduction (not heat transfer) to approximately 100° K. This means that approximately 10^8 joules were removed by gaseous and liquid nitrogen. Referring to Fig. 5, a total amount of 4200 kg (5250 liters) of liquid nitrogen was used to cool down the magnet from 240° K to 100° K. Utilizing the specific liquid requirement, I assume that we are not utilizing the sensible heat of nitrogen and, therefore, the m_{max} curves are valid.[9]

From 100° K down, the 7-W liquefier was operated as a refrigerator, with the helium gas circulated through the coil in a closed circuit. Part of the sensible heat of helium is now utilized.

The cool-down curve of the magnet system is given in Fig. 6. An average of $\sim$ 2 ... 3° K per hour cooling is about the optimum that we were able to achieve. The cooldown to 40° K was accomplished in 71 hours. Assuming that we would use supplementary liquid helium to cool down the magnet from 100° K to 4.2° K, we would require 160 kg of liquid helium, corresponding to

1280 liters (Fig. 7). Instead, cooling the magnet down from 100° K to 20° K by means of gaseous helium and from 20° K to 4.2° K by using bulk liquid helium, we used up 190 liters of helium. In Fig. 7, I assumed an average value of required helium instead of using m_{max} or m_{min} curves. This is true as we were able to utilize the sensible heat of helium only partially. The cold gas penetrates the open structure of the coil and the cool-down process is quite efficient.

To fill the container with liquid helium, approximately 480 liters of helium were used. The static helium boil-off, measured with a laminar flowmeter, was about 4 liters per hour. The steady-state helium boil-off, when the magnet had reached a central field of 9.9 T, was $\sim$ 8 liters per hour. Two pairs of current leads, with counterflow cooling, were used to carry 500 amperes to modules I, III, and IV. These leads have exhibited total losses of 4.6 liters/hour at 500-A current level (static and dynamic values). As module II was energized only to $\sim$ 60 A, total losses encountered were 0.8 liter per hour.

Referring to earlier operations of the magnet system, 14 - 16 liters of helium were evaporated per hour when only modules I ... III were energized. Recent modifications and improvements of the system allow us now to operate the magnet system continuously from our 7-watt liquefier.

The heat load imposed on the magnet refrigeration system has three origins: Heat conduction through support and electrical leads, heat radiation through the thermal insulation, and ohmic losses through the electrical leads. During magnet charging, i.e., raising and lowering the magnet current, losses are produced due to generation of eddy currents in the substrate and fluxjump resistivity in the superconductor.

The losses during magnet charging depend on the speed with which the magnetic field is increased or decreased, the conductor cross section, conductor

dimensions parallel and perpendicular to the field, the dimensions of the superconductor and the rate of twist. With the available current regulators in the cryogenics laboratory, the minimum rate at which we were able to change the the magnet current was 5 A per minute. The Max Planck coil was energized at this speed, while the current in the SLAC coil (I ... III) was increased at a rate of about 7 ... 10 A/min. This dynamic heat load resulted in an additional 3 - 5 liters per hour boil-off during magnet charging, but as it was temporary, it did not affect the long-range steady-state operation of the magnet.

The steady-state heat load of 8 liters of helium per hour for a 6-Mjoule unit having a container diameter of 1 m, is achieved, thanks to thermal shielding, careful application of superinsulation, which yielded a thermal conductivity in the order of $(1 \ldots 2) \times 10^{-6}$ W/cm ^{o}K, and liquid-nitrogen-cooled heat shields. As indicated, the heat leak and ohmic losses due to the electric leads are the largest part of the total heat load. Three pairs of leads were utilized:

(a) A pair of leads designed and built at SLAC, utilizing the sensible heat of helium gas. This pair of leads has a static heat load of 1.3 liters/hour and an ohmic loss of 1.3×10^{-3} W/A/lead at 500-A current level, as illustrated in Fig. 8, curves a_1 and a_2. These leads are essentially adequate for use at 1000 A, with 0.98×10^{-3} W/A/lead performance. They are built from two spirally-wound copper conductors, with one channel closed to helium passage by means of glass wool and only one surface cooled by the evaporated helium. These leads are efficient but costly. They were used to energize Modules I and III.

(b) A pair of leads built at SLAC by means of cooling fins. The leads are simple in design, but have a high dynamic boil-off (curve b_2 in

Fig. 8). Their static boil-off is considerably less than the other leads. These leads were used to energize Module II.

(c) The Max Planck module was energized through a pair of leads commercially acquired. These leads have a high static boil-off of ~ 2.9 liters per hour, but an ohmic loss of 2.1×10^{-3} W/A/lead at the 500-A level, which was the specified operation value. The lead performance is shown in Fig. 8, curves c_1 and c_2.

Additional losses are attributed to series connections between modules, to joints from current leads to the composite superconductor, and to internal joints within each module. The series connections may have a resistance of $\sim 10^{-7}$ ohms to 10^{-8} ohms per joint, but the total summation may add up for the balance of losses encountered.

A short note may be devoted to transfer and flashing losses when helium is transferred from 500-liter dewars to the helium container, including the magnet system. The transfer lines are rigid, evacuated, double-walled stainless steel tubes, with lengths of 2 - 3 m. They are home-built and as no superinsulation or nitrogen-cooled shields are used, losses are high and can be estimated at $\sim$ 1 watt per m length of transfer line, compared to new, highly evacuated transfer lines having loss values of < 0.3 W/m length of transfer line. As transfer lines are in use only a fraction of the operation time, this loss in the laboratory is not too important.

Additional helium in the magnet container is evaporated, when a jet of warm helium gas is blown through the transfer line into the container. This is unavoidable, as the transfer line has to be cooled from room temperature down to 4.2° K each time liquid helium is transferred from the storage dewar to the container. The flashing losses can be kept to a minimum if, at the end of the transfer line, a metallic gas breaker is installed with prevents the jet of helium from

mixing with the liquid, or if continuous helium filling is introduced. In our case, approximately 2 - 5 liters of helium are additionally evaporated each time helium is transferred.

In order to be fully equipped for all possibilities of liquid helium losses, we store approximately 1200 liters of helium in 5 dewars prior to each large-scale experiment. During the steady-state operation, the liquefier produces $\sim$ 10 liters of helium per hour, and thus the magnet steady-state operation can be extended ad libitum.

IV. SOLENOID OPERATION

The Max Planck solenoid consists of 16 pancakes of partially stabilized Nb_3Sn tape with a width of 1.27 cm. The total number of turns is 2399.* The winding inner diameter is 18.6 cm, winding outer diameter is 25.4 cm, and the coil length, 25 cm. Between pancakes, cooling passages of $\sim$ 0.3 cm width are provided. The coil is edge-cooled, and current-optimized. Three thicknesses of superconductor are used in different coil sections. The tape at the coil center has a short-sample current-carrying capacity of 700 A at 10 T.

The second conductor at the outer coil part carries 325 A at 10 T, and at the inner section, the third conductor carries 590 A at 10 T.

The short-sample characteristics of the three tapes are given in Fig. 9, curves 1, 2, and 3.

The coil was energized at various times, as oscillograms in Fig. 10 and 11 indicate.

With small backing field ($B_{ext} \cong 0.125$ T), module IV quenched at 514 A, corresponding to 4.32 T central field. With a backing field of 2 T, a central field of 6.1 T was reached.

Finally, with an external field of 5.7 T in the magnet center, module IV quenched at 512 A, generating a self field of 4.2 T. The maximum field of 9.9 T was obtained in the center of the coil system. According to the field plot in Fig. 12, this central field corresponds to a maximum field of 10.3 T at the superconductor at the inner coil radius.

This last current value is close to the short-length performance of the superconductor. Comparing the voltage-current plots of Fig. 10 and 11, we see that

---

*The information on the solenoid was kindly supplied by Dr. C. Rosner, General Electric Company, Schenectady, New York.

the insert coil, without backing field, exhibits fluxjumps. The disturbance becomes more dense at currents between 400 and 500 A. With a backing field, the disturbances are more randomly distributed, as seen in Fig. 11. Sporadic fluxjumps or more energetic flux motions are encountered.

At the last run, module IV was first energized to 450 A. While the SLAC coil was energized, the current in module IV was reduced to 245 A. As the backing field of 5.7 T was reached, the current in module IV was increased, again at a rate of $\sim$ 5 A/min, until quench current of 512 A. Subsequent operations showed that no damage to the coil occurred.

Oscillograms taken at various runs are given in Fig. 13, 14, and 15. They indicate that the quench was initiated primarily in module IV and had triggered the quench of the entire coil.

There may be several reasons why the current of 514 A at various field levels was not exceeded. After studying various possibilities, a few reasons are summarized:

(a) The current was raised in module IV at a speed of 5 - 6 A per minute. This speed is the lowest value our automatic current-control system can handle. The magnet reached 4.2 T after 100 minutes, which, according to Dr. Rosner of General Electric, is faster than they usually charge coils of this size. Due to poor thermal conductivity of Nb_3Sn at 4.2° K (2.8×10^{-4} W/cm °K), the magnetic diffusivity of the tape, $D_m \approx 0.1$ cm^2/sec, is comparable to the thermal diffusivity, $D_{th} = 0.35$ cm^2/sec. The heat generated during the field sweeping may very well create hot spots which, due to the poor heat transfer at the flat tape surface, may propagate and lead eventually to a quench.

(b) The voltage oscillograms across various pancakes indicate that the disturbance which initiated the quench occurred at the coil ends, mainly at the outer pancakes. The fact that niobium-tin tape degrades when the direction of field is perpendicular to the tape surface is known. Many measurements in coils having energies in excess of 1 Mjoule show degradation due to the radial component of the field at coil ends. Shorting strips, increase in the amount of normal material, and improvement of cooling are, in general, recommended remedies. At higher external fields, due to an improved field distribution at module IV, one may expect higher quench currents.

While the voltage across module IV exceeded 0.02 V only at random when a fluxjump occurred, the SLAC coil, based on Nb(50%)Ti composite conductor, was charted at a much faster speed with terminal voltage across the magnet exceeding 2 volts. The rate of current rise was reduced above 320 A (modules I and III), corresponding to $\sim$ 4 T to 0.75 V. Figure 16 illustrates voltage-current plots of the SLAC magnet.

(c) Module IV is installed within the SLAC magnet with its axis in a vertical position. The coolant passages are horizontal and trapped helium gas has more difficulty clearing the area of normality than in the case of vertical coolant passages where any helium gas bubbles may move much more easily. The heat flux for nucleate boiling in an open-structured magnet is $\sim$ 0.4 W/cm^2. Peak nucleate boiling heat flux for vertical surfaces is measured at 0.59 W/cm^2 and for horizontal surfaces facing downwards, only 0.19 W/cm^2. The low heat flux may have very well affected the performance of module IV.

Module IV will be part of a horizontal system, with coolant passages in a vertical position. It is possible that coil performance is improved. However, the performance of module IV is satisfactory even with the data obtained at this test. At a central field of 9.9 T, the overall current density of $1.45 \times 10^4 A/cm^2$ was reached, which is a good achievement.

ACKNOWLEDGMENTS

It is a pleasure to acknowledge the considerable work in preparation and assembly of the magnet, as well as cool-down and steady-state operation, performed by E. Tillmann of SLAC. Mr. E. Mains of General Electric Company supervised the tests at module IV and provided the voltage oscillograms (Fig. 13, 14, and 15).

I would also like to thank Professor C. Roos of Vanderbilt University, Dr. V. Scheuing of Max Planck Institute, Munich, and Dr. G. Horlitz of DESY, Hamburg, for stimulating discussions.

References

1. N. Doble et al. Proposal for a precision measurement of the Σ^+ magnetic moment. CERN/TCC 69-26. May 12, 1969.
2. H. Brechna et al. A 30-cm bore, 70-kG, superconducting Helmholtz magnet. SLAC-PUB-337. September 1967.
3. H. B. Dwight and R. W. Purssell. The force between unequal reactance coils having parallel axes. General Electric Rev. 33, 401, 1930.
4. F. W. Grover. Inductance Calculations, Working Formulas and Tables. Dover Publ. S974, New York, 1946.
5. J. C. Maxwell. Electricity and Magnetism, Vol. II, Section 701.
6. B. Weinstein. Annalen der Physik 21, 329, 1884.
7. F. W. Grover. Proc. IRE 32, 620, 1944.
8. H. Brechna. A high field 1.3-m superconducting split coil magnet with forced liquid helium cooling. SLAC-PUB-182. April 1966.
9. R. B. Jacobs. Liquid requirement for the cooldown of cryogenic equipment. Advances in Cryogenic Engineering, Vol. 8, 529-535. Plenum Press. 1962.

List of Figures

b_1. Total heat load through a SLAC lead, built of simple copper fins inside a stainless steel tube. While the static heat load is very low, the total losses, at 500-A current level, are too high.

b_2. Heat losses of lead b. At 500-A current level, the heat losses are larger than 3×10^{-3} W/A/lead. For high current performance, the lead is useless. However, it is simple and of low cost.

c_1. Total heat losses through an Avco lead commercially acquired.

c_2. The low current losses of the lead are quite high, compared to the SLAC leads. However, its optimum performance is at $\sim$ 900 A.

The best heat loss reported in literature is 10^{-3} W/A/lead. Only lead a has surpassed this value.

9. Short sample and coil performance of the GE 1.27-cm wide Nb_3Sn tape.

1. Short-sample characteristics of the Nb_3Sn tape used at the center of the MP coil.
2. Short-sample characteristics of the tape used at the coil ID on both ends of the MP coil.
3. Short-sample characteristics of the tape used at the coil outer section.
4. MP coil performance with no backing field. The coil quenched at 514 A.
5. MP coil performance with 2-T backing field.
6. MP coil performance with 4-T backing field.
7. MP coil performance with 5.7-T backing field.

10. Current-voltage characteristics of the Max Planck coil with small backing field. 1 - 2 - 4 are sporadic fluxjumps.

    The disturbances became more dense and numerous at higher field levels, until quench occurred at 514 A.

11. The current-voltage characteristics of the Max Planck coil with a backing field of 5.7 T. The current is increased, decreased, and increased again in steps. The quench occurred at 512 A.

12. Calculated total field distribution over the coil assembly. At a central field of 9.9 T, the maximum field at the MP inside diameter exceeded 10.3 T.

13. Voltage-time characteristics recorded in an 8-channel recorder. Voltage sensing leads are connected to the terminals of various double pancakes to monitor a fluxjump or the quench initiation. The fluxjump occurred at the top outer pancake. Tape advance is 0.25 cm/sec. Voltage sensitivity is 2.16 V/cm.

14. Occurrence of a fluxjump which did not quench the insert coil. Tape advancement: 0.25 cm/sec. Voltage sensitivity: 2.5 V/cm. Current in external magnet (modules I and III): 310 A. Current in insert (Module IV): 200 A.

15. Occurrence of a catastrophic fluxjump at the top end pancake, which initiated a fluxjump at 512 A, corresponding to a maximum field at the conductor of 10.3 T.

16. Voltage-current characteristic of SLAC coil modules I and III. At 300 A, the rate of current change was reduced such that the maximum terminal voltage did not exceed $\sim$ 1 volt. At 455 A, the current was held steady, while the current in the insert coil (IV) was varied. When the coil quenched, the voltage in I and III reversed to compensate for the voltage build-up in IV. (See Fig. 11).

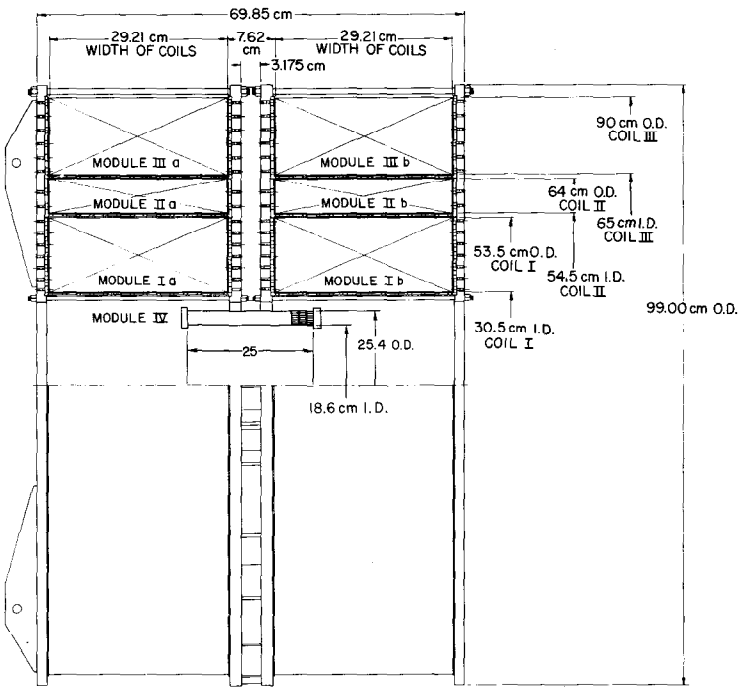

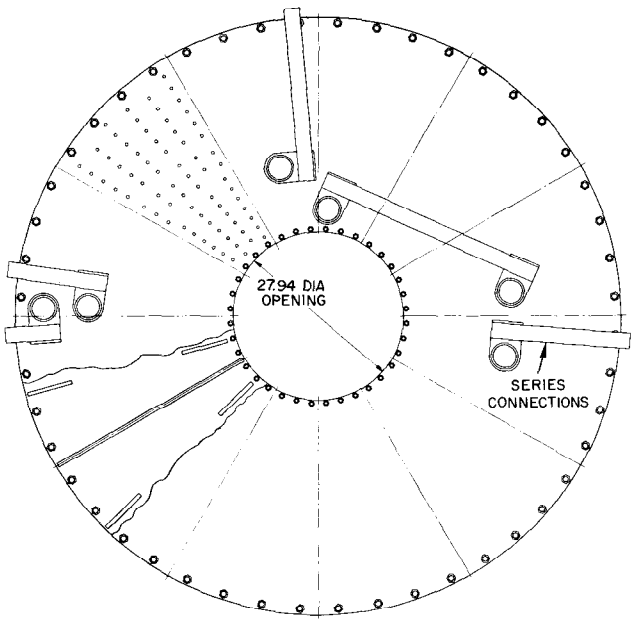

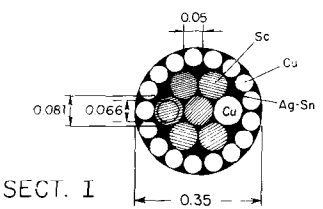

SECT. I

CABLE FOR MODULE I

30 LAYERS WITH 70 TURNS/LAYER
≅ 2070 TURNS/SECT.
$\lambda J = 3.3 \times 10^3$ Acm^{-2}

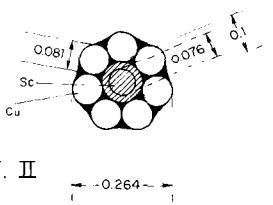

SECT. II

CABLE FOR MODULE II

14 LAYERS WITH 88 TURNS/LAYER
≅ 1200 TURNS/SECT.
$\lambda J = 3.5 \times 10^3$ Acm^{-2}

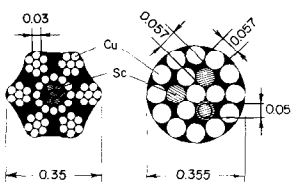

SECT. III

CABLE FOR MODULE III

32 LAYERS WITH 66 TURNS/LAYER
≅ 2126/2100 TURNS
$\lambda J = 3.4 \times 10^3$ Acm^{-2}

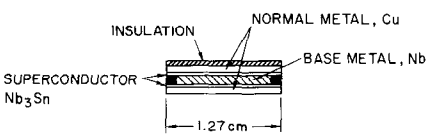

COND. FOR MODULE IV

Nb_3Sn RIBBON 1.27 cm WIDE
16 PANCAKES TOTAL 2399 TURNS
$\lambda J = 1.45 \times 10^4$ Acm^{-2}

1536C13

Fig. 1

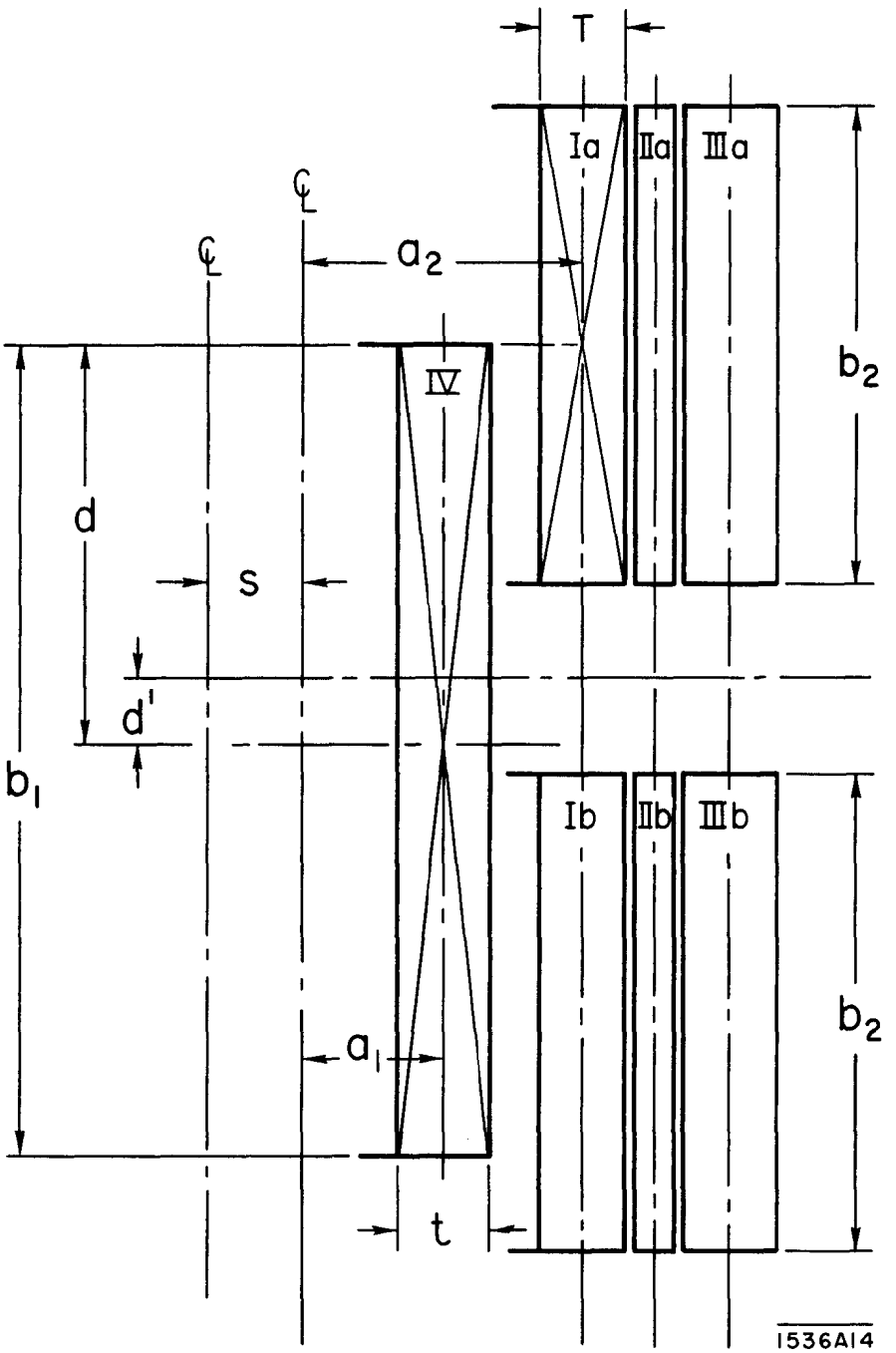

Fig. 2

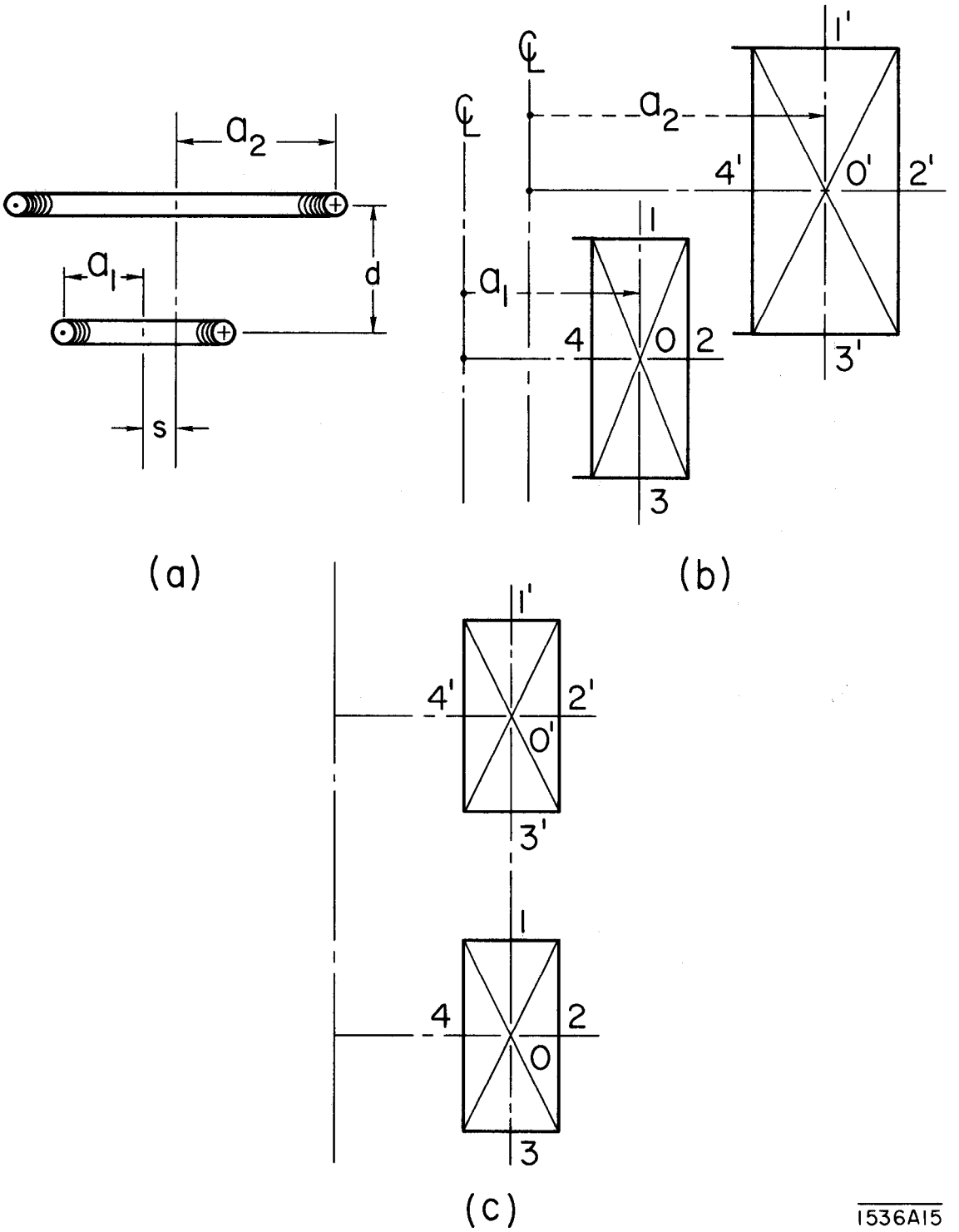

Fig. 3

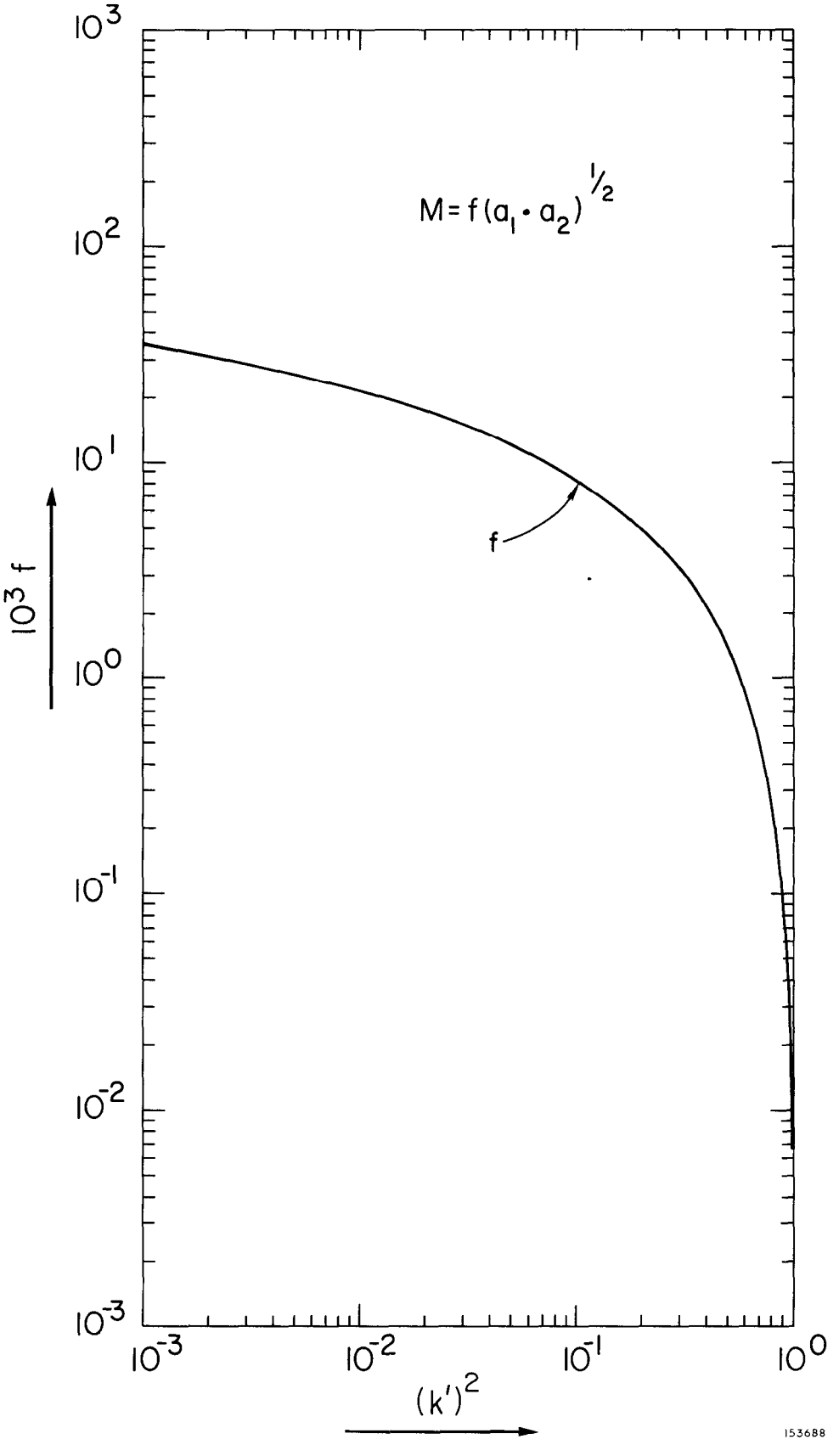
10^3
10^2
10^1
10^0
10^{-1}
10^{-2}
10^{-3}
$M = f(a_1 \cdot a_2)^{1/2}$
f
$10^3 f$
10^{-3}
10^{-2}
10^{-1}
10^0
$(k')^2$
153688

Fig. 4

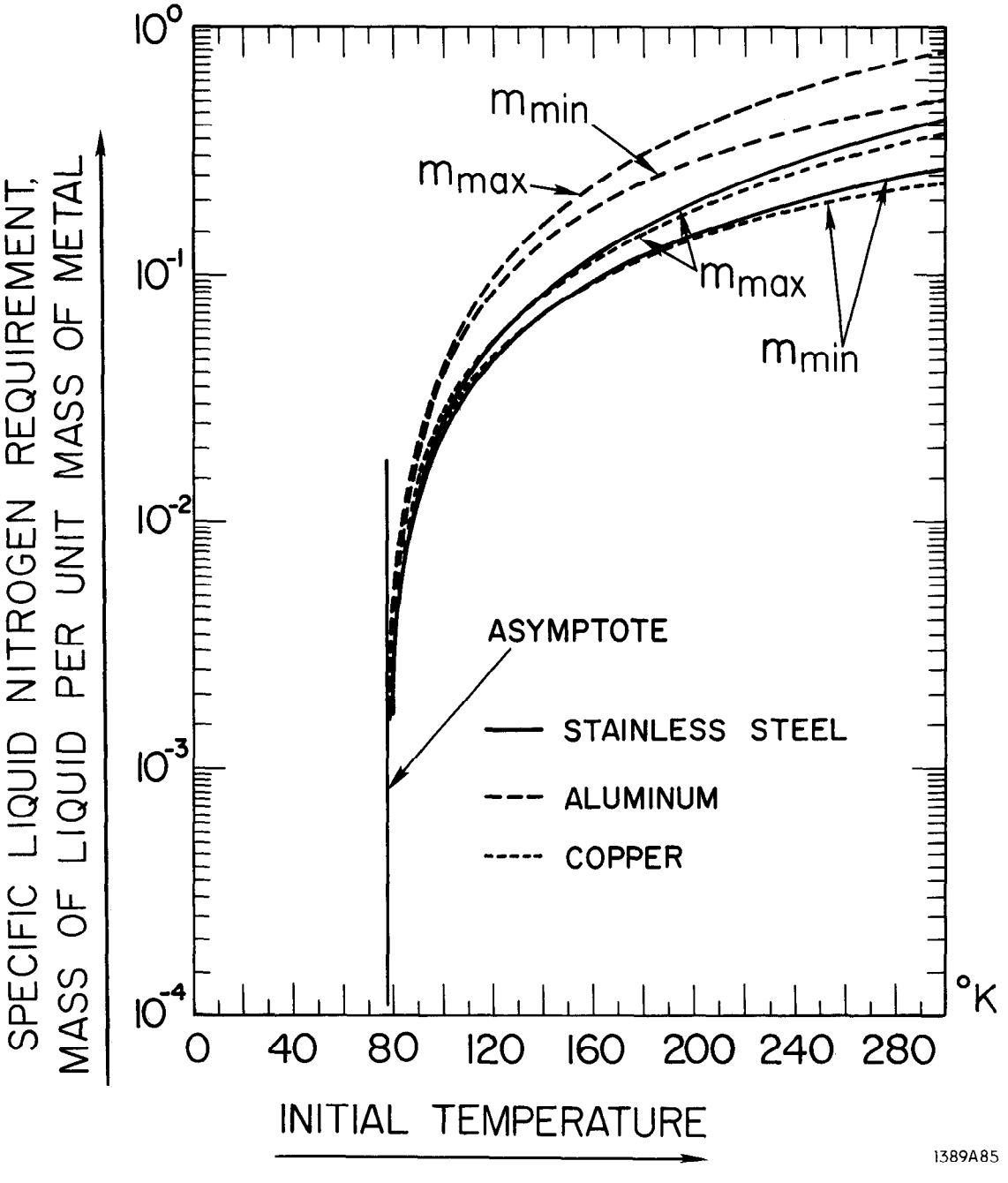
SPECIFIC LIQUID NITROGEN REQUIREMENT, MASS OF LIQUID PER UNIT MASS OF METAL
10^0
10^-1
10^-2
10^-3
10^-4
m_min
m_max
m_max
m_min
ASYMPTOTE
STAINLESS STEEL
ALUMINUM
COPPER
0
40
80
120
160
200
240
280
°K
INITIAL TEMPERATURE
1389A85

Fig. 5

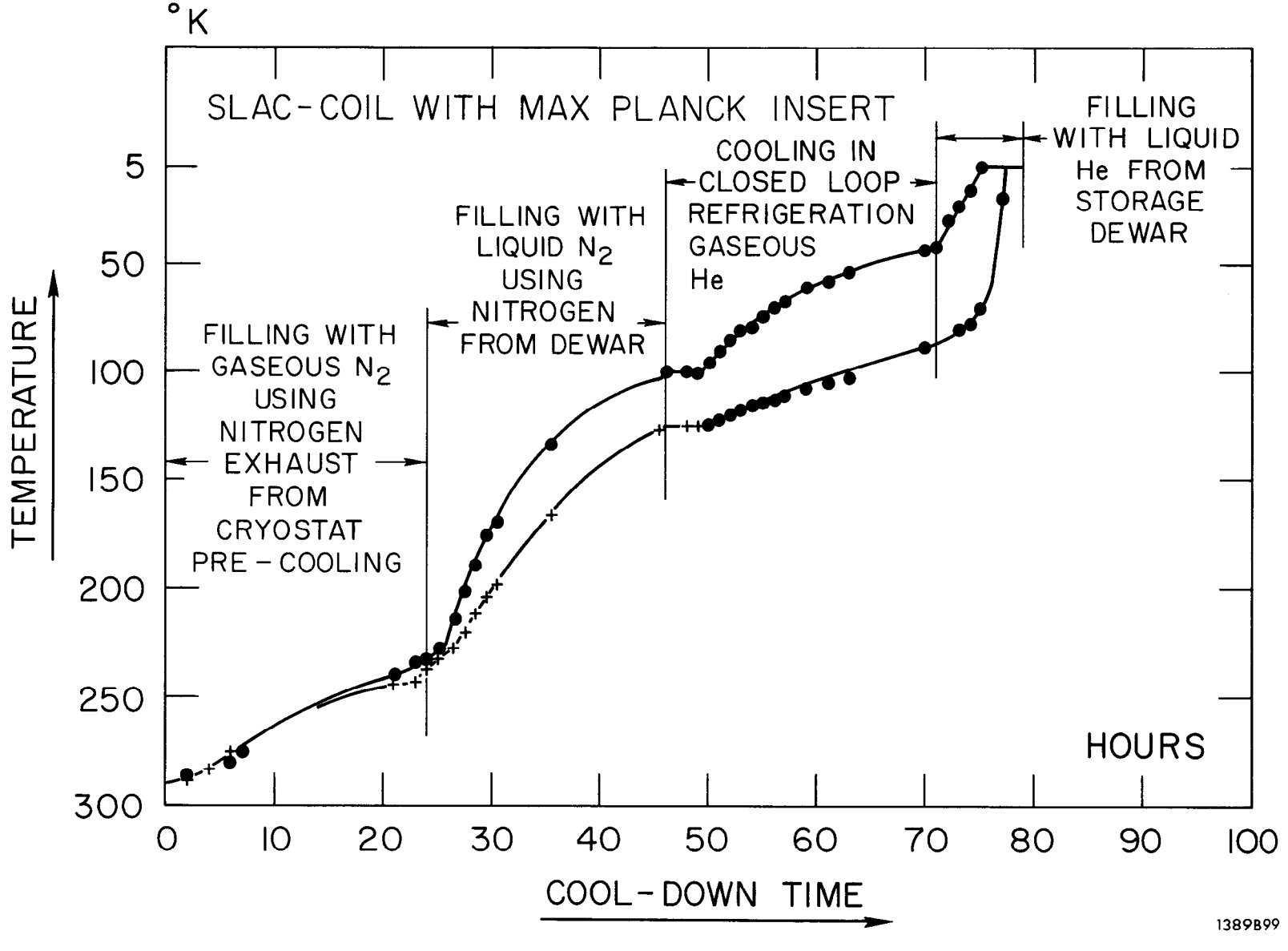
°K
SLAC-COIL WITH MAX PLANCK INSERT
FILLING WITH LIQUID He FROM STORAGE DEWAR
COOLING IN CLOSED LOOP REFRIGERATION GASEOUS He
FILLING WITH LIQUID N_2 USING NITROGEN FROM DEWAR
FILLING WITH GASEOUS N_2 USING NITROGEN EXHAUST FROM CRYOSTAT PRE-COOLING
TEMPERATURE
5
50
100
150
200
250
300
HOURS
0
10
20
30
40
50
60
70
80
90
100
COOL-DOWN TIME
1389B99

Fig. 6

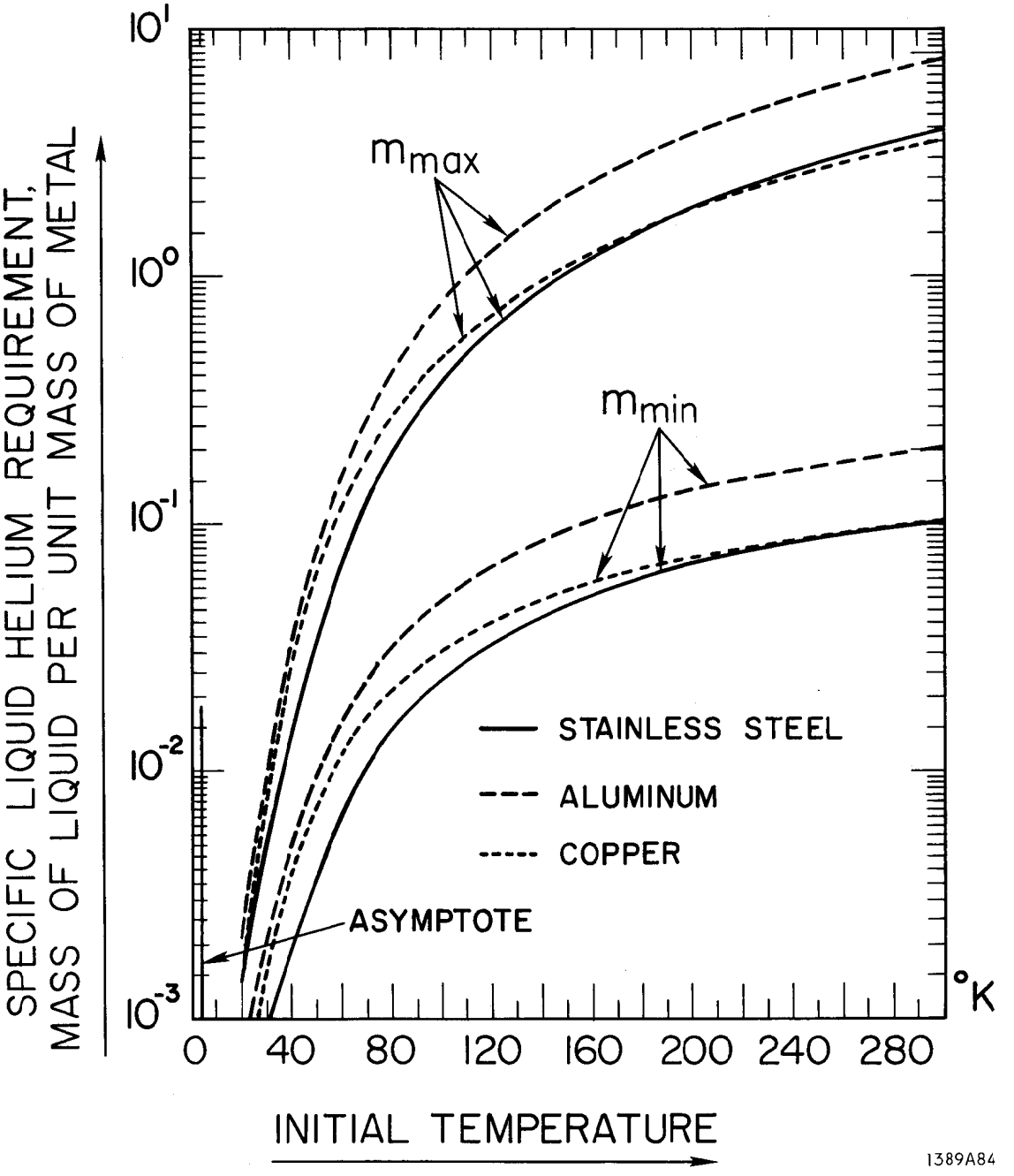
SPECIFIC LIQUID HELIUM REQUIREMENT,
MASS OF LIQUID PER UNIT MASS OF METAL
10¹
10⁰
10⁻¹
10⁻²
10⁻³
m max
m min
STAINLESS STEEL
ALUMINUM
COPPER
ASYMPTOTE
°K
0
40
80
120
160
200
240
280
INITIAL TEMPERATURE
1389A84

Fig. 7

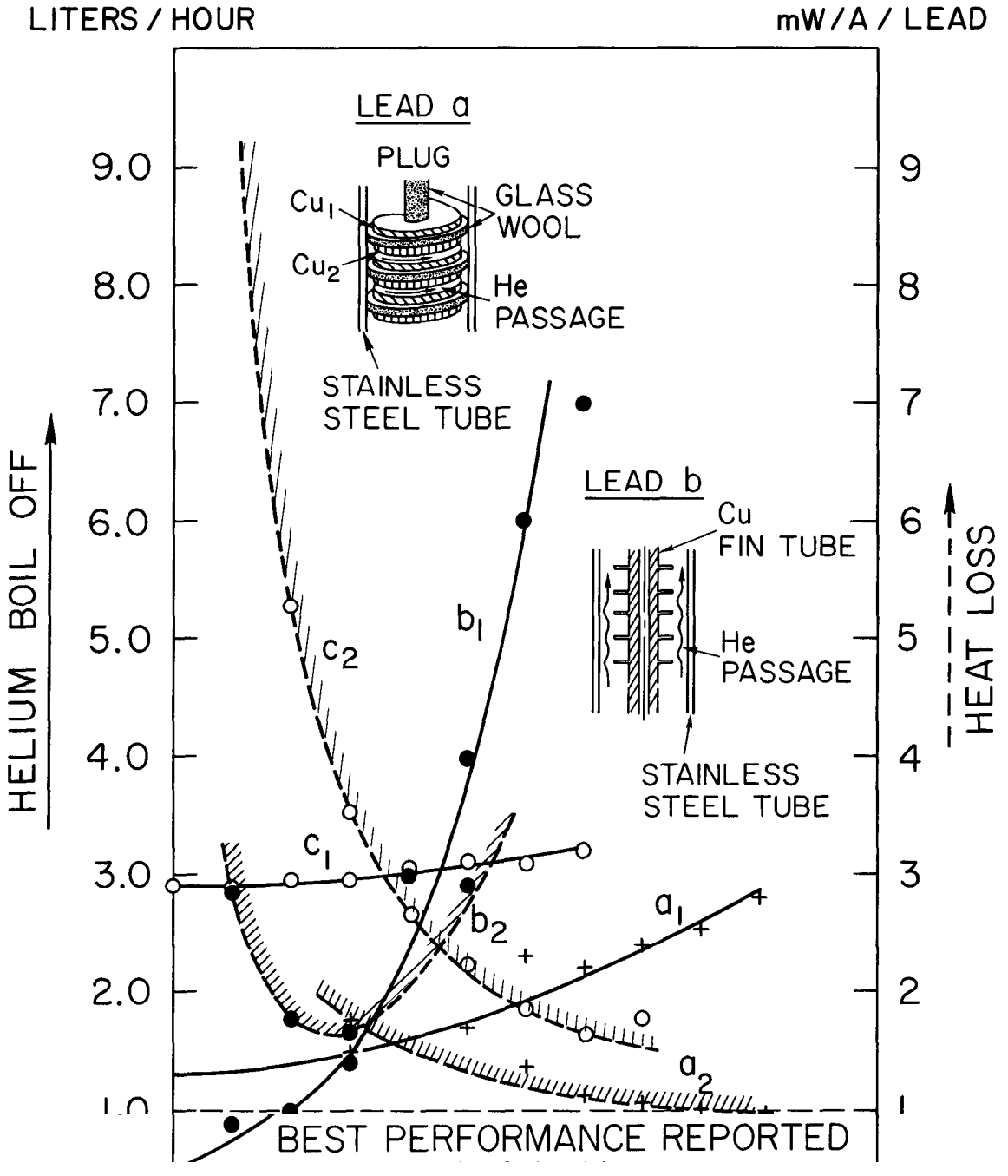
LITERS / HOUR
mW/A / LEAD
HELIUM BOIL OFF
HEAT LOSS
9.0
8.0
7.0
6.0
5.0
4.0
3.0
2.0
1.0
9
8
7
6
5
4
3
2
1
LEAD a
PLUG
Cu1
Cu2
GLASS WOOL
He PASSAGE
STAINLESS STEEL TUBE
LEAD b
Cu FIN TUBE
He PASSAGE
STAINLESS STEEL TUBE
c2
b1
c1
b2
a1
a2
BEST PERFORMANCE REPORTED

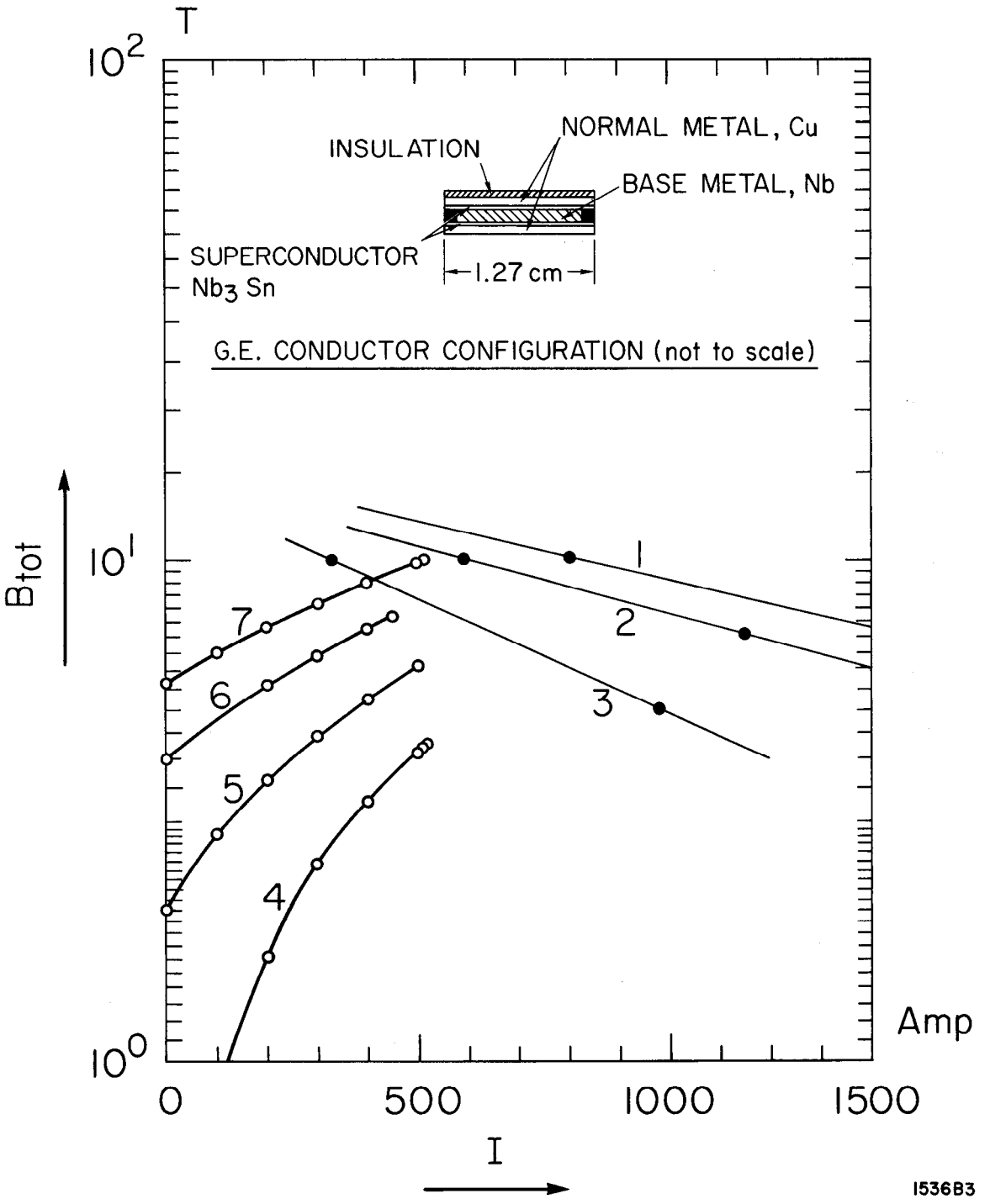
T
10^2
INSULATION
NORMAL METAL, Cu
BASE METAL, Nb
SUPERCONDUCTOR
Nb_3Sn
1.27 cm
G.E. CONDUCTOR CONFIGURATION (not to scale)
B_{tot}
10^1
10^0
1
2
3
4
5
6
7
0
500
1000
1500
Amp
I
1536B3

Fig. 9

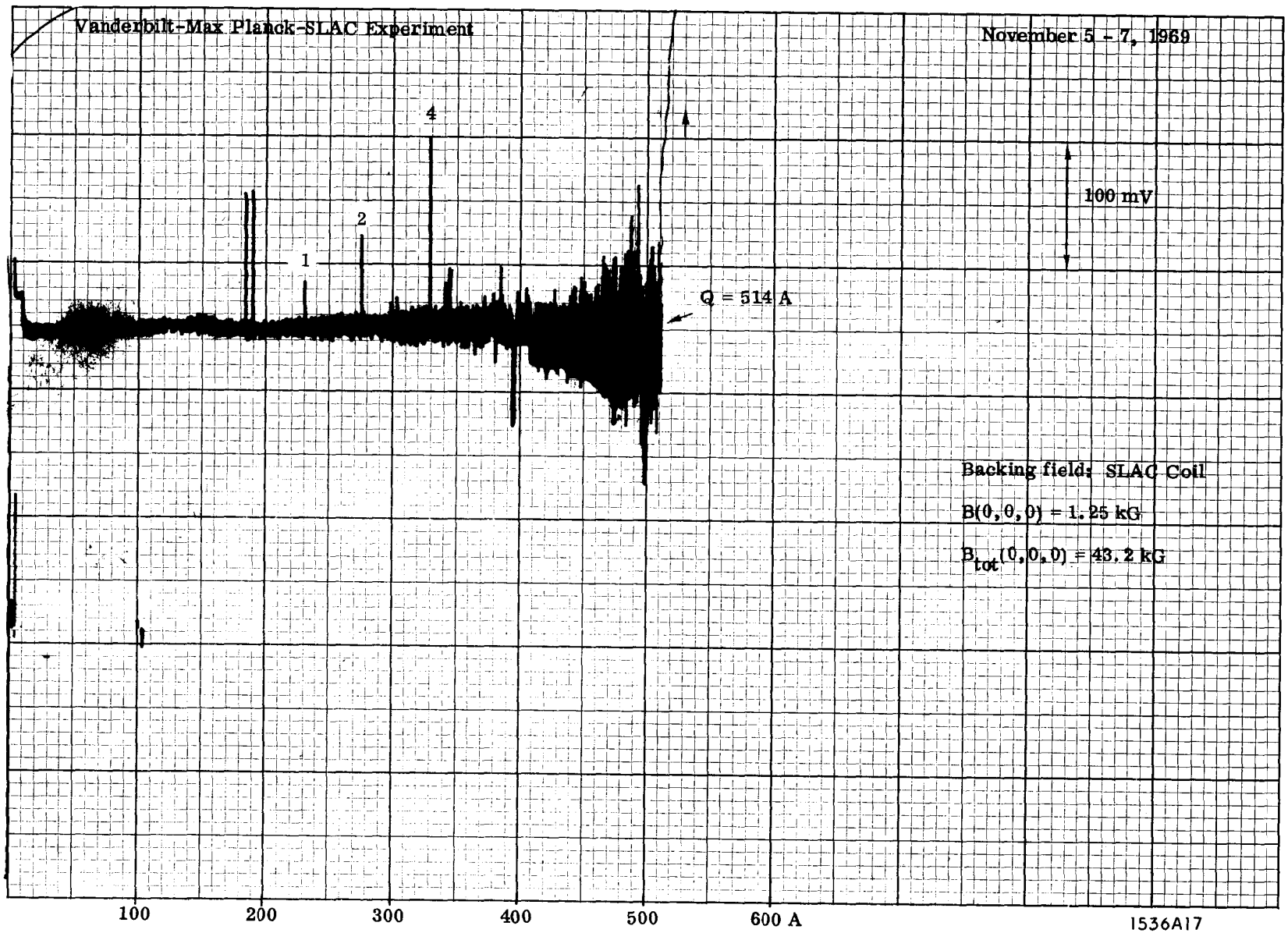
Vanderbilt-Max Planck-SLAC Experiment
November 5 - 7, 1969
4
2
1
100 mV
Q = 514 A
Backing field: SLAC Coil
B(0,0,0) = 1.25 kG
B_{tot}(0,0,0) = 43.2 kG
100
200
300
400
500
600 A
1536A17

Fig. 10

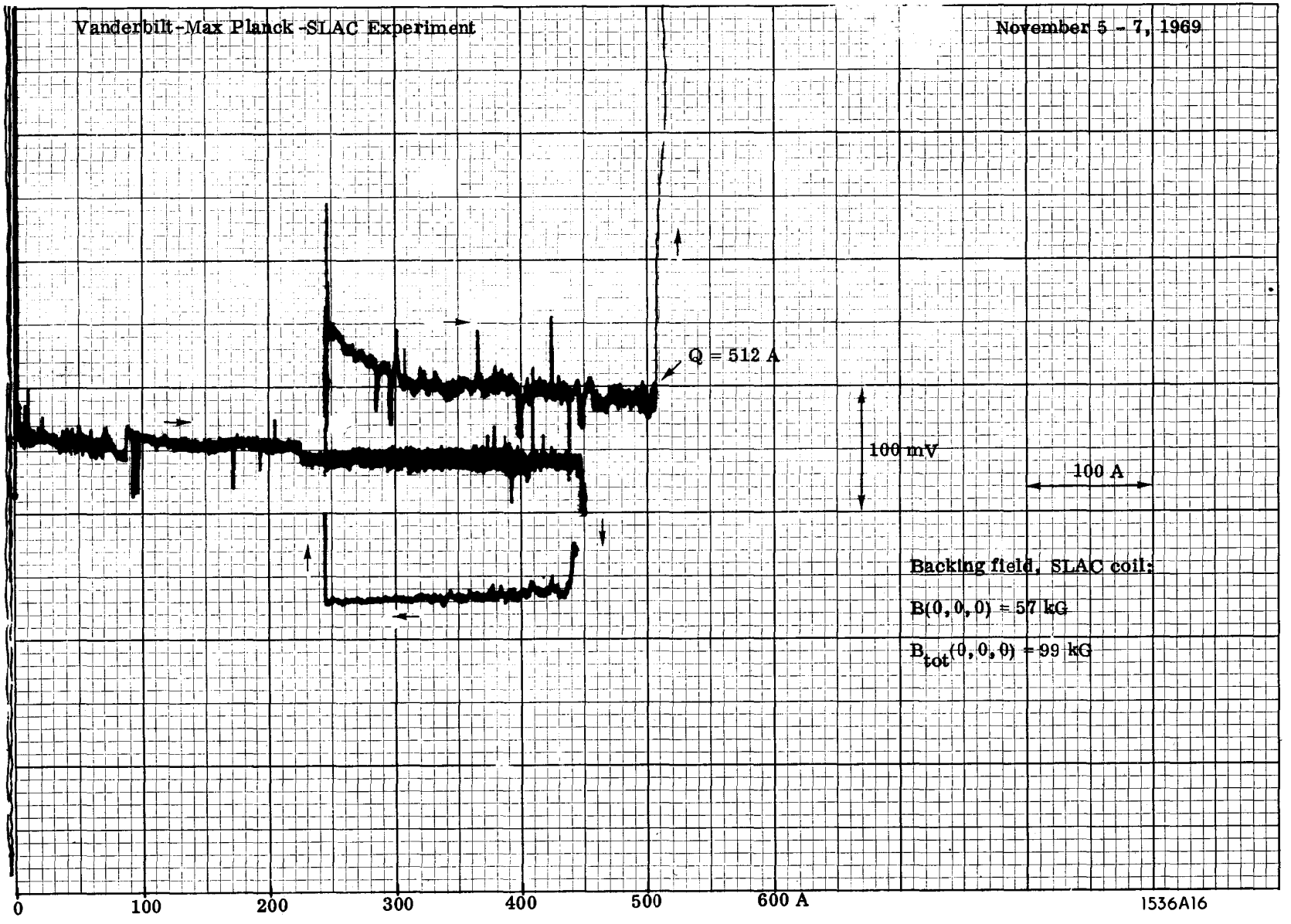
Vanderbilt-Max Planck-SLAC Experiment
November 5 - 7, 1969
Q = 512 A
100 mV
100 A
Backing field, SLAC coil:
B(0, 0, 0) = 57 kG
B_{tot}(0, 0, 0) = 99 kG
0
100
200
300
400
500
600 A
1536A16

Fig. 11

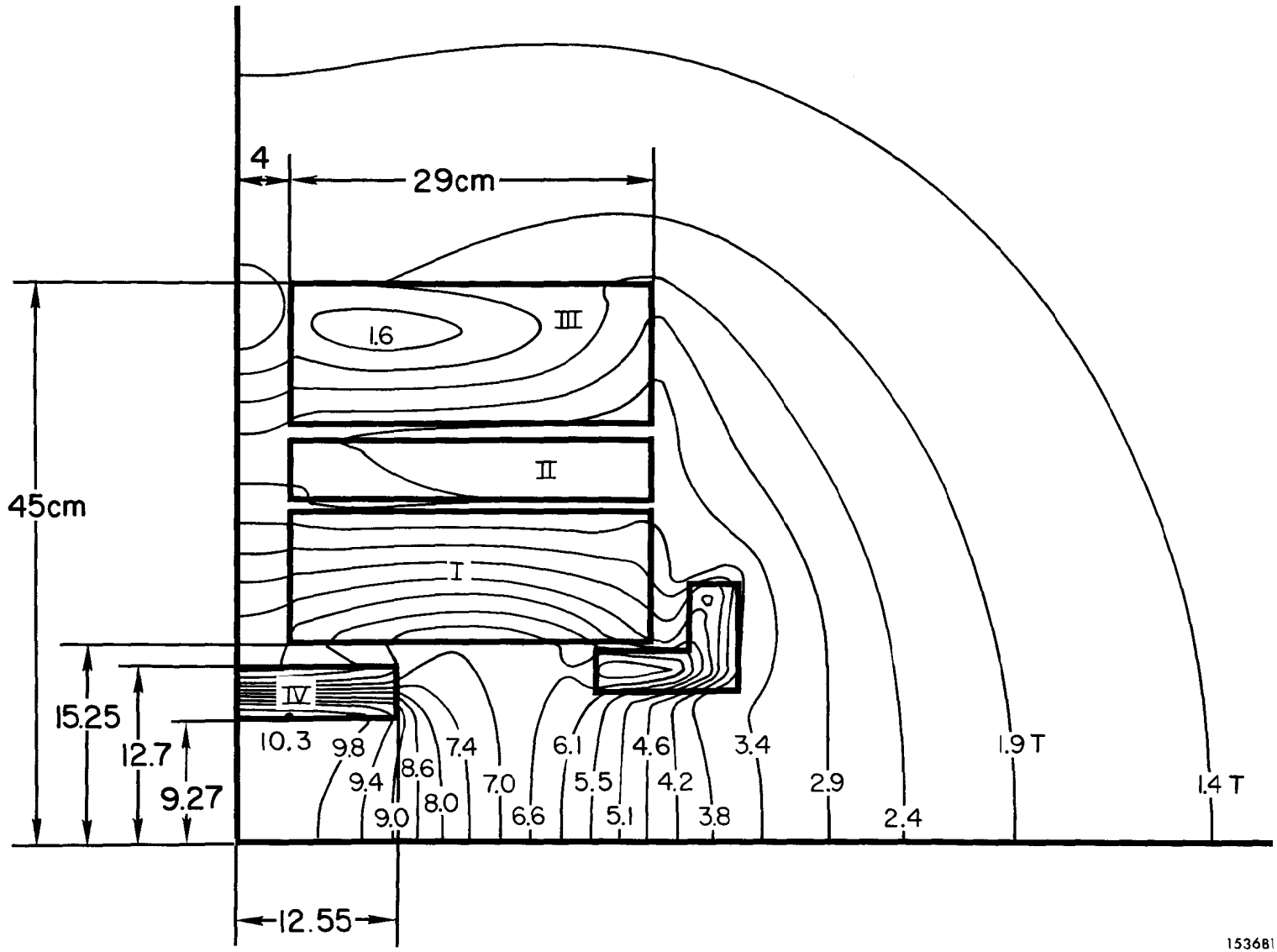
4
29cm
45cm
15.25
12.7
9.27
12.55
III
II
I
IV
1.6
10.3
9.8
9.4
9.0
8.6
8.0
7.4
7.0
6.6
6.1
5.5
5.1
4.6
4.2
3.8
3.4
2.9
2.4
1.9 T
1.4 T
153681

Fig. 12

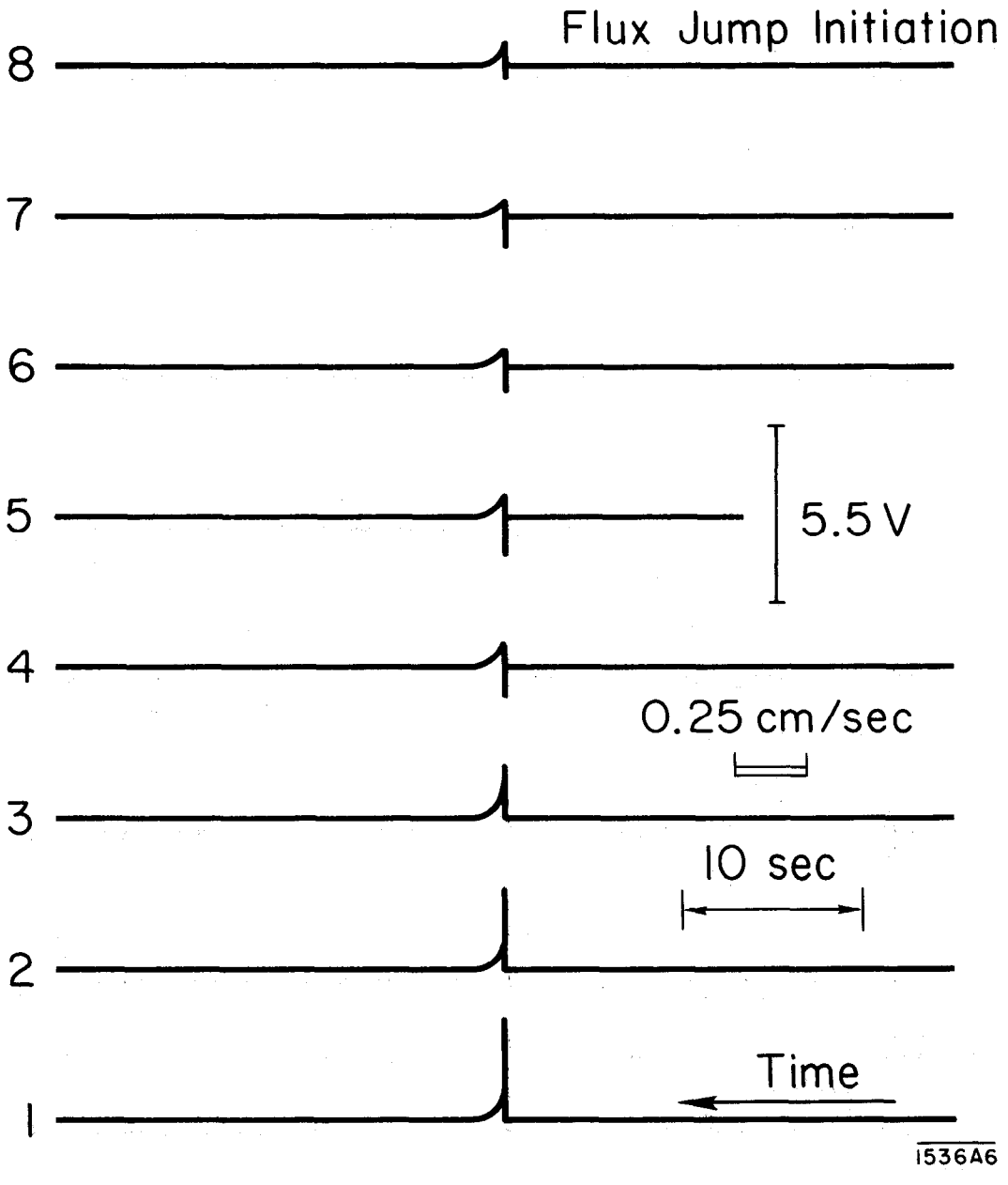
Flux Jump Initiation
8
7
6
5
5.5 V
4
0.25 cm/sec
3
10 sec
2
Time
1
1536A6

Fig. 13

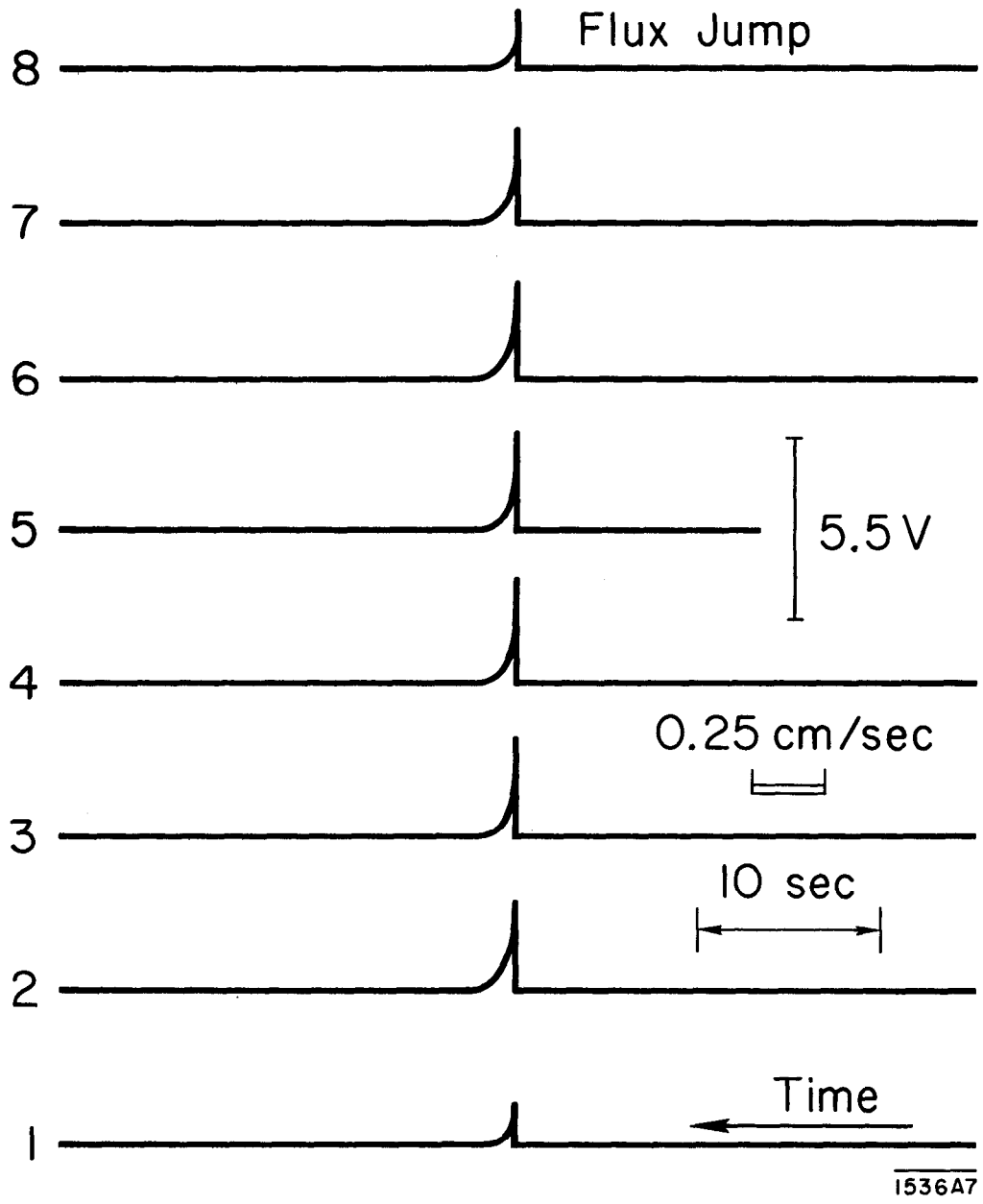

Fig 14

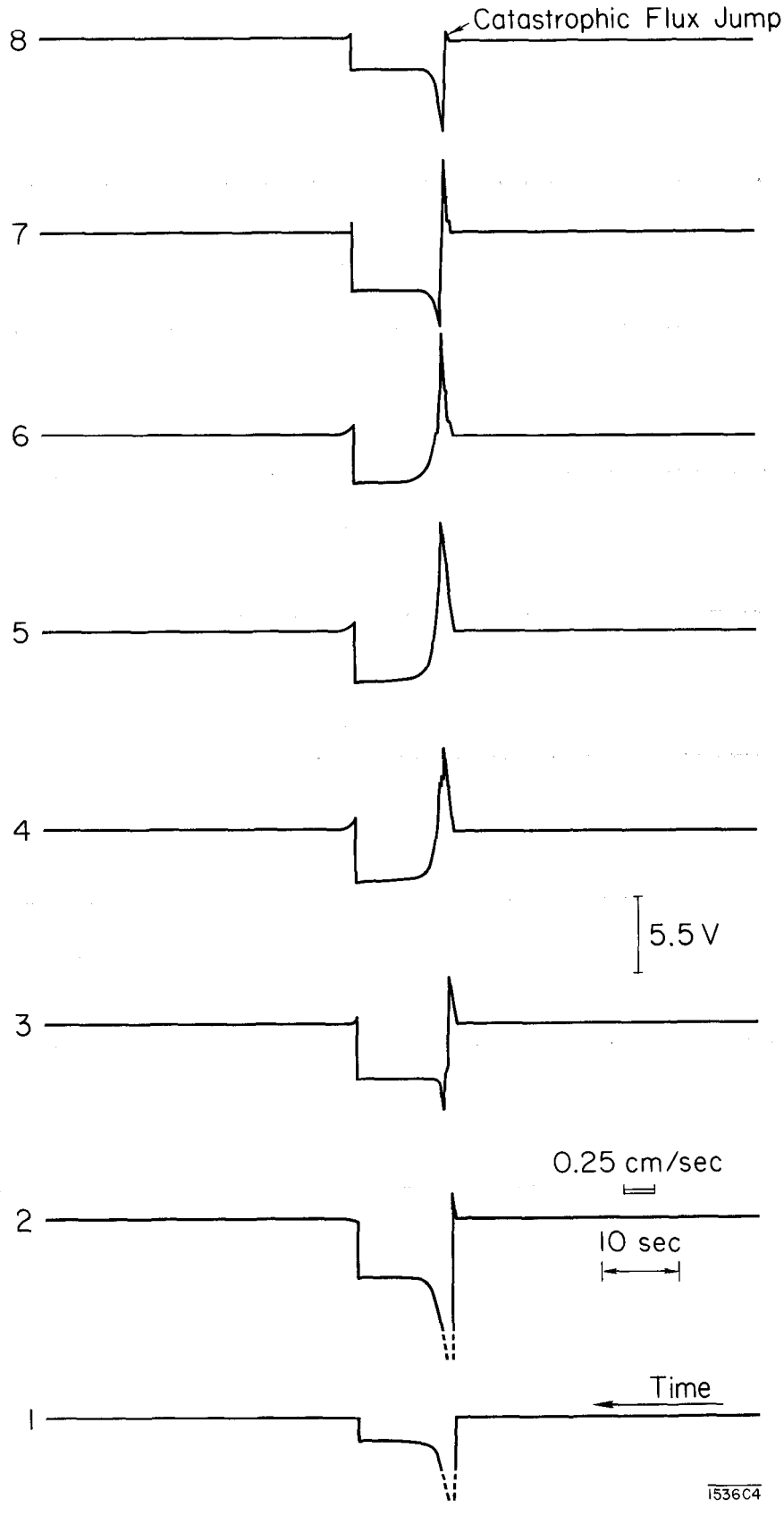
Catastrophic Flux Jump
8
7
6
5
4
5.5 V
3
0.25 cm/sec
2
10 sec
Time
1
1536C4

Fig. 15

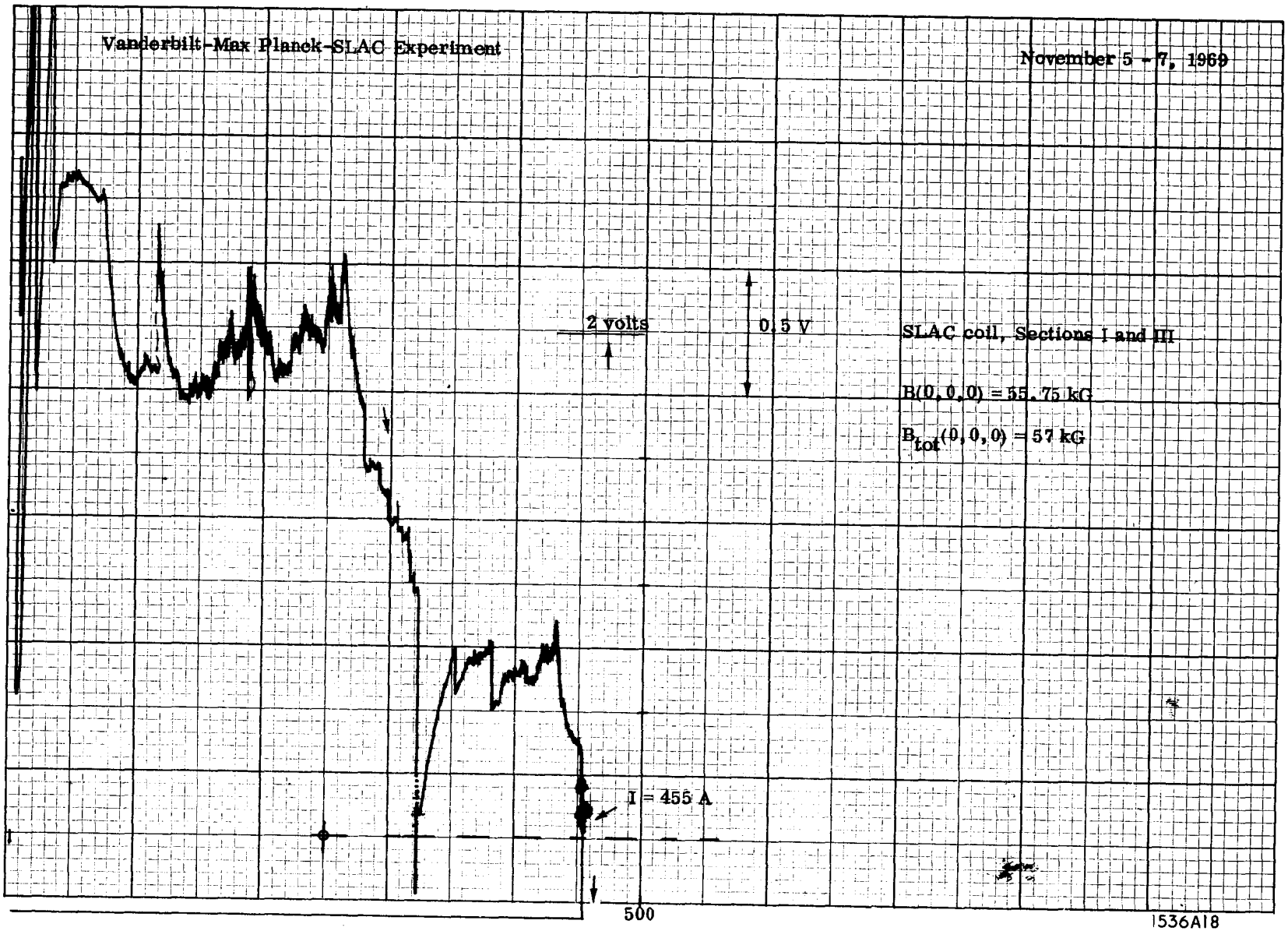
Vanderbilt-Max Planck-SLAC Experiment
November 5 - 7, 1969
2 volts
0.5 V
SLAC coil, Sections I and III
B(0, 0, 0) = 55.75 kG
B_{tot}(0, 0, 0) = 57 kG
I = 455 A
500
1536A18

Fig. 16